Available online at www.sciencedirect.com
ScienceDirect
Geomorphology 80 (2006) 178–198
GEOMORPHOLOGY
www.elsevier.com/locate/geomorph

Spatially and temporally distributed modeling of landslide susceptibility

Pece V. Gorsevski [a,*], Paul E. Gessler [a], Jan Boll [b], William J. Elliot [c], Randy B. Foltz [c]

[a] Department of Forest Resources, University of Idaho, Moscow, ID 83844, USA
[b] Department of Biological and Agricultural Engineering, University of Idaho, Moscow, ID 83844, USA
[c] Rocky Mountain Research Station, USDA Forest Service, 1221 South Main Street, Moscow, ID 83843, USA

Received 29 April 2005; received in revised form 13 February 2006; accepted 15 February 2006
Available online 23 March 2006

Abstract

Mapping of landslide susceptibility in forested watersheds is important for management decisions. In forested watersheds, especially in mountainous areas, the spatial distribution of relevant parameters for landslide prediction is often unavailable. This paper presents a GIS-based modeling approach that includes representation of the uncertainty and variability inherent in parameters. In this approach, grid-based tools are used to integrate the Soil Moisture Routing (SMR) model and infinite slope model with probabilistic analysis. The SMR model is a daily water balance model that simulates the hydrology of forested watersheds by combining climate data, a digital elevation model, soil, and land use data. The infinite slope model is used for slope stability analysis and determining the factor of safety for a slope. Monte Carlo simulation is used to incorporate the variability of input parameters and account for uncertainties associated with the evaluation of landslide susceptibility. This integrated approach of dynamic slope stability analysis was applied to the 72-km^2 Pete King watershed located in the Clearwater National Forest in north-central Idaho, USA, where landslides have occurred. A 30-year simulation was performed beginning with the existing vegetation covers that represented the watershed during the landslide year. Comparison of the GIS-based approach with existing models (FSmet and SHALSTAB) showed better precision of landslides based on the ratio of correctly identified landslides to susceptible areas. Analysis of landslide susceptibility showed that (1) the proportion of susceptible and non-susceptible cells changes spatially and temporally, (2) changed cells were a function of effective precipitation and soil storage amount, and (3) cell stability increased over time especially for clear-cut areas as root strength increased and vegetation transitioned to regenerated forest. Our modeling results showed that landslide susceptibility is strongly influenced by natural processes and human activities in space and time; while results from simulated outputs show the potential for decision-making in effective forest planning by using various management scenarios and controlling factors that influence landslide susceptibility. Such a process-based tool could be used to deal with real-dynamic systems to help decision-makers to answer complex landslide susceptibility questions.

Keywords: Landslide susceptibility; Distributed modeling; Monte Carlo simulation; GIS; Factor of safety

1. Introduction

Landslides are natural geologic processes that constantly evolve and reshape the Earth's surface. The recent intensification of land-use changes has raised the level of landslide susceptibility, particularly

* Corresponding author.
E-mail address: peceg@uidaho.edu (P.V. Gorsevski).

0169-555X/$ - see front matter © 2006 Elsevier B.V. All rights reserved.
doi:10.1016/j.geomorph.2006.02.011

in mountainous regions. Landslides that initiate in steep mountainous terrain are a major concern to land-use managers worldwide. Human activities, such as urban expansion, road-building, and deforestation increase the potential for landslides and result in adverse impacts to the environment (Chung et al., 1995; Burton and Bathurst, 1998). In the US alone, landslides cause an estimated annual average economic cost of $1.5 billion (Glade, 1998). In Japan, annual losses are $2 billion and in Italy, annual losses are more than $ 2.6 billion (Blöchl and Braun, 2005). Worldwide in the 20th century the Asian continent has experienced the most landslide events (220 reported), the Americas reported the most deaths and injuries (25,000+) while Europe had the highest average damage per single event ($23 million) (CRED, 2006).

Landslides result from interdependent spatio-temporal processes, including hydrology (rainfall, evapotranspiration, and groundwater), vegetation surcharge (weight of vegetation), root strength, soil condition, bedrock, topography, and human activities (Wu and Sidle, 1995). For instance, change in the forest cover, particularly from clear-cut harvesting, affect processes of soil infiltration and evapotranspiration as well as vegetation surcharge and root strength, which collectively tend to decrease slope stability and increase the risk of landsliding. In steep soil-mantled landscapes, shallow landslide occurrences exert a tremendous downstream impact by transporting sediment and debris from higher to gentler slopes. Downstream effects from landslides result in decreased water quality, loss of fish spawning habitat, and debris jams that may break during peak flows, thereby scouring channels and destroying riparian vegetation.

Mapping areas susceptible to landslides is essential for land-use management and should become a standard tool to support land management decision-making. Consequently, the need for methodologies which guide managers to choose the best management strategies while minimizing impacts from land-use activities in vulnerable slope areas, is increasing. Many methods and techniques have been proposed to evaluate where or when landslides are most likely to occur, some using Geographic Information Systems (GIS) (Ward et al., 1982; Carrara, 1983; Okimura and Ichikawa, 1985; Hammond et al., 1992; Montgomery and Dietrich, 1994; Carrara et al., 1995; Mark and Ellen, 1995; Wu and Sidle, 1995; Duan and Grant, 2000; Gorsevski, 2002; Ayalew and Yamagishi, 2005; Guzzetti et al., 2005). Quantitative techniques include: stability ranking based on criteria such as slope, parent material, and elevation (McClelland et al., 1997; Moreiras, 2005); statistical models linking environmental attributes using spatial correlation (Carrara, 1983; Carrara et al., 1991; Chung et al., 1995; Chung and Fabbri, 1999; Dhakal et al., 2000; Gorsevski, 2002; Gorsevski et al., 2000; Gorsevski et al., 2003; Gorsevski and Gessler, 2003; Gorsevski et al., 2005; Ayalew and Yamagishi, 2005), and process models that combine the infinite slope equation and hydrological components (Montgomery and Dietrich, 1994; Wu and Sidle, 1995; Gorsevski, 2002). Regionally, methods like the Forest Service method (FSmet; McClelland et al., 1997) and SHALSTAB (Dietrich and Montgomery, 1998) are used to identify landslide susceptibility. However, these methods usually do not address influences of temporally varying precipitation, vegetation dynamics, uncertainty associated with input parameters, as well as various scenarios that may be implemented through an extended management period. Outputs from these methods are limited to only a snapshot of spatial prediction of landslide susceptibility and may not account for dynamic processes.

Prediction of landslide susceptibility based on static environmental factors and/or the existence of steady-state conditions appears to be simplistic (Wu and Sidle, 1995; Gorsevski, 2002; Gorsevski et al., 2003). Relatively static environmental factors (i.e., elevation, slope, aspect, and topographic curvatures) exhibit negligible changes in their state through time, and differ from dynamic factors such as climatic or human activities, which tend to alter landslide susceptibility through time. However, spatial differences do exist in both environmental factors. To predict the spatial and temporal patterns of areas susceptible to landslides, a distributed approach is needed that incorporates varying precipitation intensity, soil depth, vegetation (species, age, density), and root strength. Wu and Sidle (1995) developed and tested a dynamic, distributed, physically based slope stability model (dSLAM). Their model includes the infinite slope model (Hammond et al., 1992; Montgomery and Dietrich, 1994; Wu and Sidle, 1995), a kinematic wave groundwater model, and a dynamic vegetation growth model including continuous changes in root cohesion and vegetation surcharge. The dSLAM model uses individual hourly rainfall hyetographs for event simulations or long series of random rainstorms for long-term simulations. Slope stability is simulated using the spatial distribution of the factor of safety (FS), which is the ratio of resisting and driving forces favoring failure. Application of dSLAM is feasible only in areas with sufficient information on the spatial variability of parameters such as soil depth, root strength, and vegetation surcharge. Because detailed

mapping of such parameters in forested and mountainous areas is rare, an alternative representation of the uncertainty and variability inherent in these parameters is needed.

Therefore, in this paper we present a different dynamic, distributed landslide susceptibility model, which is capable of predicting and mapping areas susceptible to landslides and explicitly takes account of uncertainty in input variables due to measurement logistics. We integrate the Soil Moisture Routing (SMR) model (Boll et al., 1998; Frankenberger et al., 1999) with the infinite slope equation and Monte Carlo simulation. In this integrated approach, input parameters that are highly variable in space and time (e.g., soil depth, root strength, and vegetation surcharge) are expressed as mathematical functions such as uniform and log-normal probability distributions and then sampled and statistically evaluated using Monte Carlo simulation (Hammond et al., 1992; Burrough and McDonnell, 1998; Malczewski, 1999; Duan and Grant, 2000). Monte Carlo simulation reflects the effects of uncertainties associated with the input parameters by evaluating a large number (i.e., $n=1000$) of possible scenarios and simulating the range of probable values for each input parameter.

The integrated approach (SMR/FS/Monte Carlo) that was developed fully within the ARC/INFO GRID module was used to simulate the hydrology of the Pete King watershed in central Idaho and estimate the spatial and temporal distribution of the factor of safety. This new approach is intended to improve upon regional methods such as FSmet and SHALSTAB. Three specific objectives are addressed: (1) to examine if the spatial prediction of landslide susceptibility using the integrated approach yields better accuracy or precision than spatial prediction using existing models (FSmet, SHALSTAB); (2) to examine if the probability of slope failure changes for each year over a 30-year simulation (temporal change); and (3) to examine if the probability of slope failure changes spatially over a 30-year simulation. A 30-year modeling period was chosen because of the management period for harvesting tree species, but this period is flexible and users could select other time periods based on interests for use. The 30-year period also allows forest classes with at least a 20-year period to transition to different forest classes and captures the trends driven by root strength on slope stability. To evaluate the first objective, the criteria used for judging which approach yields better accuracy or precision uses a ratio of correctly identified landslides to areas classified as susceptible. To evaluate the second and the third objectives, the spatio-temporal results generated by the integrated approach are evaluated.

2. Overview of the SMR/FS/Monte Carlo approach

The following sections detail the components for the SMR/FS/Monte Carlo approach, and briefly describe the existing FSmet and SHALSTAB models that were tested and compared in the study area.

2.1. Soil moisture routing model

The SMR model used here (Boll et al., 1998; Frankenberger et al., 1999) is a simple distributed water balance model running on a daily time step, which predicts saturation-excess overland flow occurring at any point in a watershed using a raster GIS. The cell size of the raster data is optional but the optimal dimensions range from 10 to 30 m (Boll et al., 1998). The data sets used by the SMR model combine climate data, a digital elevation model, multi-layered soils, and land use data. The SMR model calculates the water balance at each time step (e.g. daily) for each grid-cell using the following equation:

$$D_i \frac{\mathrm{d}\theta_i}{\mathrm{d}t} = P(t)_i - \mathrm{ET}(t)_i + \frac{\sum Q_{\mathrm{in}.i} - \sum Q_{\mathrm{out}.i}}{A} - L_i - R_i \quad (1)$$

where i is the cell address; t is time; D_i is depth to restrictive layer for each cell i; θ_i is the volumetric soil moisture content of the cell; $P(t)_i$ is precipitation (rain and snowmelt) for time t and cell i; $\mathrm{ET}(t)_i$ is actual evapotranspiration for time t and cell i; $\sum Q_{\mathrm{in}.i}$ is lateral inflow from surrounding upslope cells; $\sum Q_{\mathrm{out}.i}$ is lateral outflow to surrounding downslope cells; L_i is drainage out of the surface soil layers to bedrock for cell i; R_i is surface runoff for cell i; and A is the area of the cell. Daily precipitation and lateral flow from uphill cells are the inputs to each cell in the model, while lateral flow to downhill cells, percolation into the subsurface, evapotranspiration, and surface runoff are the outputs from each cell.

Precipitation consists of all moisture inputs, including rainfall and snowmelt. Precipitation occurring when the mean daily temperature is below 0 °C is assumed to be snow. Snow is assumed to remain until the mean daily temperature is above 0 °C. Snowmelt is modeled with the degree-day method (U.S. Army Corps of Engineers, 1960):

$$M = mt + k, \quad \text{if } t > 0\ ℉\mathrm{C} \quad (2)$$

where M is snowmelt (cm/day); t is the average daily temperature; m is the snowmelt factor (0.23 cm/°C in forested and 0.27 cm/°C in non-forested areas); and k is a constant (0 in forested and 1.22 cm in non-forested areas).

Evapotranspiration for cell i (ET_i) is calculated as a function of daily potential evapotranspiration, vegetation, and soil moisture content in the cell. When the moisture content is below the wilting point, there is no evapotranspiration. Evapotranspiration takes place only when the matric potential is at 1/3 bar or wetter, and a linear relationship is assumed (Thornthwaite and Mather, 1955) between the wilting point and 1/3 bar.

$$ET_i = PET(ET/PET)_i c_i \tag{3}$$

where PET is potential evapotranspiration; (ET/PET)i is the ratio of actual to potential evapotranspiration based on soil moisture content; and c_i is a vegetation coefficient that varies throughout the year for each vegetation class.

Subsurface lateral flow is calculated for each cell using Darcy's Law, by approximating the hydraulic gradient by the land slope, β_i, at each cell:

$$Q_{out.i} = wK(\theta_i)D_i\beta_i \tag{4}$$

where $Q_{out.i}$ is lateral outflow from the cell; D_i is depth to restrictive layer for each cell i; w is width of each cell; and $K(\theta_i)$ is lateral hydraulic conductivity of the soil profile at cell i as a function of the soil moisture content. When the average θ_i is less than the field capacity, θ_{fc}, the following equation holds:

$$K(\theta_i) = K_s \exp\left(-\alpha \frac{\theta_s - \theta_i}{\theta_s - \theta_r}\right) \tag{5}$$

where K_s is saturated hydraulic conductivity; θ_r is residual moisture content; θ_s is porosity; and a is a constant (Bresler et al., 1978). If the soil moisture content is above the field capacity, the hydraulic conductivity is calculated as.

$$K(\theta_i) = (K_s - K(\theta_{fc}))\left(-\alpha \frac{\theta_i - \theta_{fc}}{\theta_s - \theta_{fc}}\right) + K(\theta_{fc}) \tag{6}$$

Lateral flow is calculated by a multiple flow path algorithm (Quinn et al., 1991) that divides the lateral flow among all downslope cells based on the steepest drop and distance between the cells:

$$P_{ij} = \frac{(Z_i - Z_j)/L_j}{\sum_{j=1}^{n} [(Z_i - Z_j)/L_j]} \tag{7}$$

where P_{ij} is the portion of the total flow out of cell i routed to a neighboring cell j; Z_i and Z_j is the elevation of cell i and its neighbor j, respectively; L_j is the distance from cell i to neighbor j; and n is the number of downslope neighbors of cell i.

Stream flow calculated by SMR is the sum of surface runoff generated in the watershed, subsurface lateral flow into the stream, and a portion of the water stored in the bedrock reservoir each day, which represents the base flow. SMR was calibrated using observed stream flow and Monte Carlo simulation. Water table depth in each cell was used in the infinite slope equation to calculate the factor of safety.

2.2. Infinite slope equation and factor of safety

The infinite slope equation has been applied to calculate FS in many slope stability investigations because of its simplicity (Hammond et al., 1992; Montgomery and Dietrich, 1994; Wu and Sidle, 1995). FS is defined as the ratio of resisting (shear strength) to driving forces (shear stress):

$$FS = \frac{C_r + C_s\cos^2\alpha[q_0 + \gamma(D - D_w) + (\gamma_{sat} - \gamma_w)D_w]\tan\phi}{\sin\alpha\cos\alpha[q_0 + \gamma(D - D_w) + \gamma_{sat}D_w]} \tag{8}$$

where α is slope angle of the ground surface; D is total soil thickness; D_w is saturated soil thickness; C_r is tree root strength expressed as cohesion; q_0 is tree surcharge; C_s is soil cohesion; ϕ is effective internal angle of friction; γ is moist soil unit weight; γ_{sat} is saturated soil unit weight; and γ_w is water unit weight. A slope with a FS > 1 is considered stable, while a slope with a FS < 1 is unstable. In addition, vegetation surcharge, the weight of vegetation that adds to the gravitational force on a slope, needs to be considered. The calculation of a single FS is deterministic and does not incorporate uncertainty and variability in the parameters. For instance, a slope with a FS of 0.8 may not fail due to model input uncertainties. Introducing probabilistic analysis into the calculation of FS can provide an estimate of the probability of slope failure, which may be calculated as the number of occurrences of FS < 1 at a particular location, divided by the total number of runs.

2.3. Monte Carlo simulation

This study attempts to characterize and incorporate uncertainty into the calculation of the probability of slope failure using Monte Carlo simulation. Table 1 shows the parameters that were considered to vary with their

Table 1
Stochastic variables, their probability distributions, and references that suggested the distributions

Stochastic variable	Probability distribution	Reference
Soil depth	Uniform	Ward et al. (1982), Duan and Grant (2000)
Soil cohesion	Uniform	Ward et al. (1982), Duan and Grant (2000)
Internal friction angle	Uniform	Ward et al. (1982), Duan and Grant (2000)
Root strength	Lognormal	Hammond et al. (1992)
Vegetation surcharge	Uniform, and dynamic with age	Ward et al. (1982), Duan and Grant (2000)

assumed probability distributions (Ward et al., 1982; Hammond et al., 1992; Duan and Grant, 2000). After running a large number of trials (at least 1000 random simulations) to eliminate variations within the resulting probability density functions (PDFs), statistical properties (e.g., mean and standard deviation) for each entity were calculated (Burrough and McDonnell, 1998). For instance, a soil inventory describing upper and lower limits of soil depth was represented by a PDF with a uniform distribution function with a rectangular shape as described by previous work (e.g., Hammond et al., 1992).

2.4. FSmet and SHALSTAB

Landslide susceptibility outputs were generated using two existing models: FSmet (McClelland et al., 1997) and SHALSTAB (Dietrich and Montgomery, 1998). FSmet represents a heuristic approach specifically developed for the Clearwater National Forest (CNF), while SHALSTAB is a physically based model including the infinite slope equation of the Mohr–Coulomb failure law and steady-state shallow subsurface flow (O'Loughlin, 1986).

The FSmet was developed using the following attributes: geology, elevation, aspect, slope gradient, landform, and a database of landslide event locations from 1995 to 1996 (described below). The geology was derived from parent material groupings from the Clearwater Land System Inventory (FS-CNF, 1983) at a cartographic scale of 1:100,000 and included: the Idaho batholith (primarily granitics), border (high grade metamorphic rocks), belt (weakly metamorphic rocks), Columbia River basalts (layered volcanic materials), and alluvium (materials from surface erosion and deposition). Elevation, aspect, and slope were extracted from 1:24,000 topographic maps in conjunction with stereo pair imagery. Landform groups included breaklands, mountain slopes, mountain ridges, gentle hills, mass wasting landforms, and valleys. The landform groups were also extracted from the Clearwater Land System Inventory at a cartographic scale of 1:100,000 which are mainly described by slope steepness and landform derivation processes. However, the outputs from FSmet are compiled by intersecting areas that meet the criteria of slopes greater than 60%, parent materials of schist and granitics, and elevations below 1400 m. The restriction to 1400 m elevation is based on the fact that during the landslide events in the winter of 1995–1996, the snowpack existed at higher elevations so cooler temperatures did not contribute to rain-on-snow events that cause landsliding. The original landslide database used by McClelland et al. (1997) for the development of the FSmet was also used for our study to permit the comparison of landslide susceptibility.

SHALSTAB was implemented as an ArcView extension to generate landslide susceptibility output using a digital elevation model (DEM), soil bulk density, and friction angle as inputs. The soil bulk density and friction angle were set to 1860 kg/m^3 and 32°, respectively, which are the same as the mean values derived by the Monte Carlo simulation and used in the integrated SMR/FS/Monte Carlo approach. SHALSTAB's one-step option (Dietrich and Montgomery, 1998) was used to calculate the critical value of the ratio of steady-state effective precipitation (rain minus evapotranspiration; q) to transmissivity (the ground's subsurface ability to convey water downslope; T) needed to generate a landslide. The q/T ratio has dimensions of $(L/T)/(L^2/T)$ or L^{-1}. A large q/T ratio implies that the soil approaches saturation, and a high susceptibility of slope failure. Because q/T is always <1, $\log(q/T)$ is reported. SHALSTAB classifies landslide susceptibility as: "unconditionally stable," "potentially unstable," and "unconditionally unstable". Unconditionally stable elements are predicted not to fail even when saturated, while unconditionally unstable are predicted to fail even when dry. Potentially unstable elements are associated with values of $\log(q/T)$ ranging from -1.9 to -3.4 incremented by -0.3 where divisions within the range of values are user-imposed. Areas with large absolute values of $\log(q/T)$ represent the least stable areas, whereas areas with small absolute values of $\log(q/T)$ represent the most stable areas. We applied arbitrary cut-off values of greater than -2.2 to represent "unconditionally stable" areas, greater than -2.8 to represent the mid-point of "potentially unstable" areas, and greater than -3.1 to represent "unconditionally unstable" areas. The landslide database from 1995 to 1996 used by McClelland et al. (1997) was also used for comparison.

3. Application of the modeling approach

3.1. Study area

The integrated modeling approach and the existing models were tested on the Pete King watershed in the CNF in north-central Idaho (Fig. 1). Pete King is a 72-km^2 drainage, with elevation ranging from 450 to 1592 m and slopes ranging between 0° and 45°. Annual precipitation averages 970 mm. Much of this precipitation falls as snow during winter and spring. Peak stream discharge occurs in late spring and early summer. Soils are variable but typically shallow and well drained and primarily derived from the Belt Supergroup (gneiss and schist) and Idaho Batholith parent materials (FS-CNF, 1983). The vegetation across the elevational gradient includes Grand fir (*Abies grandis*), Douglas fir (*Pseudotsuga menziesii*), Subalpine fir (*Abies lasiocarpa*), Western redcedar (*Thuja plicata*), Western white pine (*Pinus monticola*), and various shrubs and grasses with short growing seasons particularly at high elevations.

The Pete King watershed was affected by landslide events that occurred during the winter of 1995–1996. Landslides were assessed and mapped through aerial reconnaissance flights and field inventory in July 1996. Aerial photography was acquired at a scale of 1:15,840 followed by photo interpretation between October 1996 and February 1997 (McClelland et al., 1997). Landslide locations identified by initial aerial and field reconnaissance were transferred to 1:24,000-base quadrangle maps to be used by the field crew. About 40% of the total landslides identified from aerial photos were visited and verified. In 1999, the authors verified the GIS data quality by comparing two sets of aerial photos, one was acquired in August 1995 prior to the 1995 November storm, and the other was acquired in July, 1996 following the landslide events and was used for the original landslide inventory. The presence or absence of a landslide was represented as a (30-m) grid coverage with values of 1 for presence and 0 for absence for each grid cell. The initiation area or the scar of each landslide was represented as a point. A total of 45 landslides (with

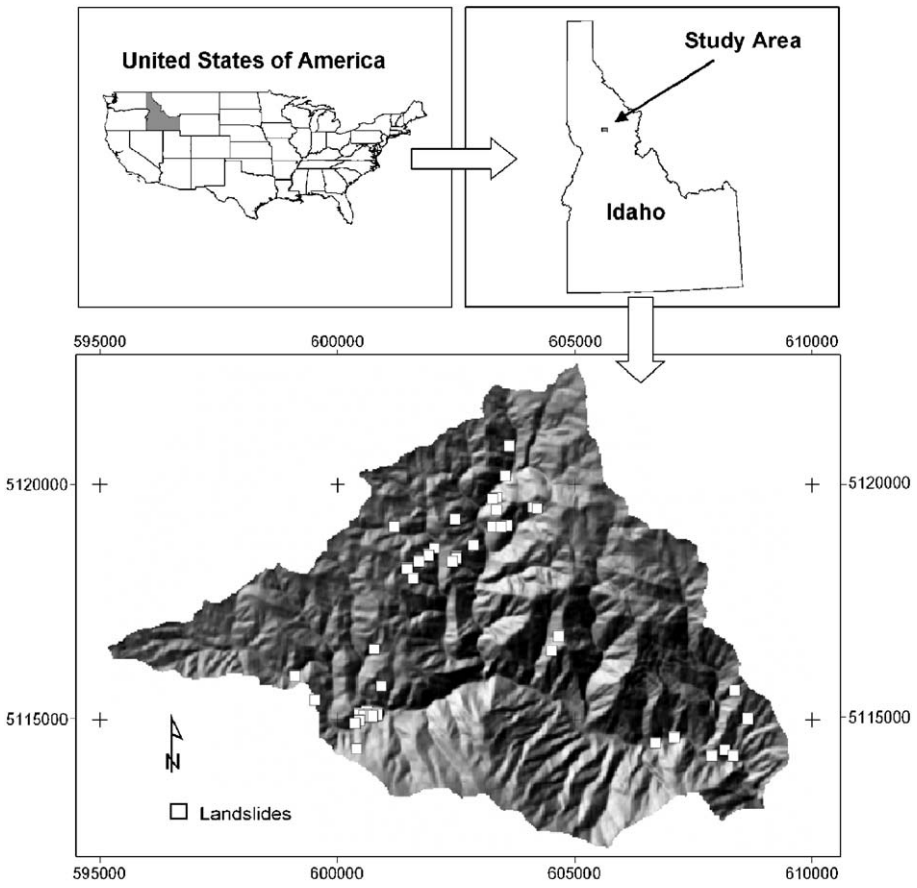

Fig. 1. Distribution of landslides over the Pete King watershed during the winter 1995–1996 storm events. The projection is Universal Transverse Mercator (UTM) using the American Datum of 1927.

a failure surface in the soil mantle) with a minimal size of 10 cubic yards (7.65 m^3) were recorded. These include landslides initiated as a consequence of natural processes as well as land-use activities. The watershed has experienced a number of road failures in 1970, 1978, and 1987. Other historical data suggest that 2582 ha of forest have been harvested, 256 km of roads have been constructed, together covering 36.3% of the watershed, and in 1934, a large fire burned 34% of the watershed (Hickey, 1997). During the last 60 years, approximately 70% of the watershed has experienced some form of disturbance such as roads, harvest, and fire (Hickey, 1997).

3.2. SMR model input

In order to corroborate the outputs from the SMR model with field measurements, the daily stream flow to the primary outlet of the modeled watershed, generated by SMR using climatic data, was compared against the observed stream flow. To capture model responses associated with an extreme year when actual landslides occurred, the model was calibrated for a period of 14 months in the year of the landslide events (from July 1, 1995 to September 1, 1996) and then used to simulate a period of 30 years of stochastically derived data using a climate generator program (CLIGEN; Nicks et al., 1995). Input for the SMR model consisted of the 7.5-min U.S. Geological Survey DEM (nominally 30 m resolution), land cover derived from a Landsat Thematic Mapper image classification

Table 2
Soil physical parameters used in the SMR model

Soil parameter	Soil layer			Reference
	A	E	B	
(Lateral) Saturated hydraulic conductivity (cm/day)	160	30	50	
(Restricting layer) Saturated hydraulic conductivity (cm/day)	0.04	0.04	0.04	
Saturated moisture content (cm^3/cm^3)	0.58	0.42	0.52	Flanagan and Livingston (1995)
Field capacity (cm^3/cm^3)	0.37	0.27	0.28	Flanagan and Livingston (1995)
Permanent wilting (cm^3/cm^3)	0.11	0.08	0.09	Saxton et al. (1986)

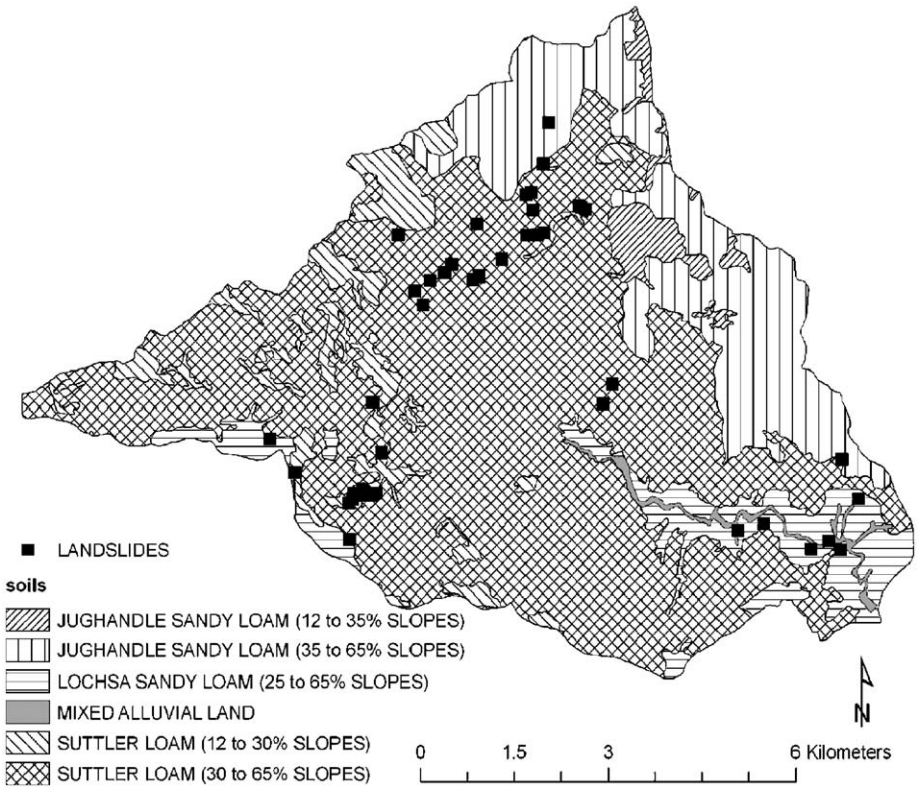

Fig. 2. Soil types in the Pete King watershed.

Table 3
Lower and upper boundaries of horizon depths (cm) categorized by CTI quartiles that were used to model spatially distributed soil depths for the Pete King watershed

Soil horizon	Compound Topographic Index (CTI)			
	Quartile 1	Quartile 2	Quartile 3	Quartile 4
A	0–15	0–20	0–25	0–30
E	15–46	20–66	25–86	30–106
B	46–87	66–107	86–127	106–147

(30 m resolution), observed daily weather data for the calibration period, stochastically generated daily weather data for the simulation period, and soils data at a 1:24000 scale from the Soil Survey Geographic Database (SSURGO) (USDA-NRCS, 2001).

We assumed that the soil texture for the entire study area is loam (Fig. 2), and the soil profile is divided into three horizons (A, E, and B). These assumptions simplify the derivation of the soil physical parameters (Table 2) that were not available through the soil survey for the study area. The depths of the profile horizon boundaries were extracted from SSURGO and later adjusted when we calibrated the SMR model (described below). The depth of each horizon inferred by SSURGO is 0 to 30 cm for the A horizon, 30 to 106 cm for the E horizon, and 106 to 147 cm for the B horizon. Soil

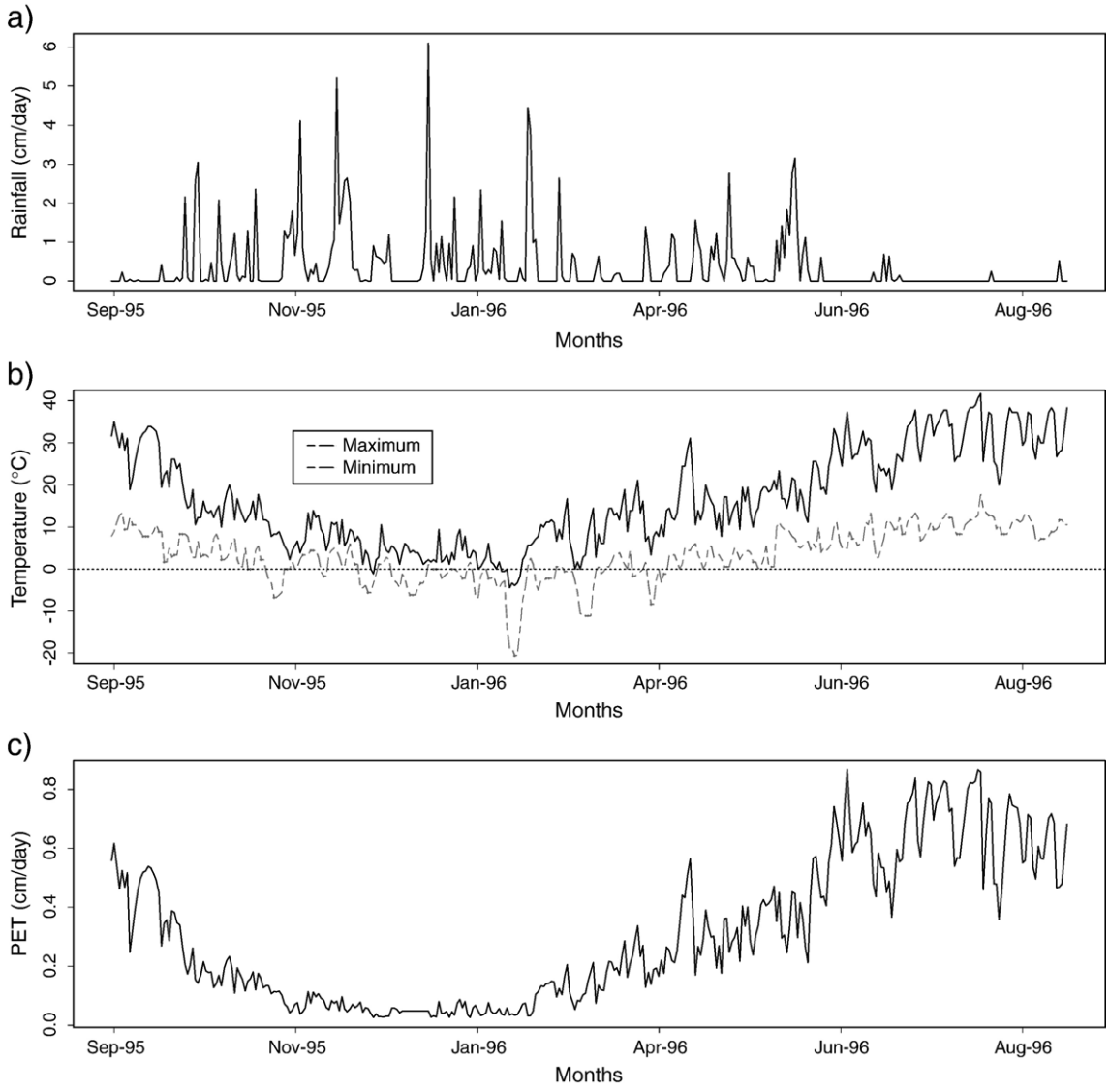

Fig. 3. Climate data used in the SMR model. (a) Hyetograph for the Pete King watershed including the storm events in 1995–1996; (b) observed maximum and minimum temperature; and (c) potential evapotranspiration estimated by Hargreaves and Samani's (1985) method.

moisture data were taken from Flanagan and Livingston (1995) and Saxton et al. (1986) (Table 2). Empirical approaches (e.g. regressions) were taken when independent variables such as sand, clay, organic matter, bulk density, cation exchange capacity (CEC), and soil depth were estimated from the SSURGO data. To represent soil depths across the Pete King watershed more realistically, the compound topographic index (CTI) was calculated, because it is highly correlated with overall soil depth (Dietrich et al., 1995; Gessler et al., 1995, 2000). The CTI, also referred to as the steady-state wetness index (Beven and Kirkby, 1979; Moore et al., 1991), is defined as:

$$\mathrm{CTI} = \ln(A_s/\tan\beta) \quad (9)$$

where A_s is specific catchment area in m^2 and β is the slope angle in degrees. A distribution of CTI for the watershed, divided evenly into four quartile classes with different sets of minimum and maximum soil depth values, were used in the Monte Carlo simulation. Table 3 shows the minimum and maximum horizon depth values that were used to represent the CTI and soil depth relationships. The values were guided by SSURGO but were slightly adjusted to characterize steep hillslopes with shallow soil depths and low quartile CTI values as well as valley-bottoms with deep soil depths and high quartile CTI values.

Assuming a uniform frequency distribution between the minimum and maximum values (Table 1), the average CTI/depth for each cell in each quartile was described by using 1000 random simulations.

Daily weather data (NOAA, 2001) from the Fenn Ranger Station (46°06′12″N, 115°33′55″W; elevation 487 m) were used for the calibration period (Fig. 3). Daily weather inputs (NOAA, 2001) were minimum and maximum temperatures and total precipitation. The temperature was adjusted for elevation by a lapse rate of 0.64 °C per 100 m. A total of 20 missing values for the precipitation data and 13 missing values for the temperature data for 1995–1996 were interpolated based on distance and elevation differences from nearby weather stations (Dworshak Hatchery, Kamiah, and Kooskia).

Potential evapotranspiration was estimated using the Hargreaves method (Hargreaves and Samani, 1985). A cloud-free Landsat Thematic Mapper image from 1995 was used to extract vegetation classes for the study area to assign evapotranspiration coefficients as well as the vegetation surcharge and root strength parameters for the FS calculations (Table 4). The land cover was classified using an unsupervised clustering algorithm, which incorporated an iterative process of randomly selecting cluster centers. Simple three vegetation cover types, clear-cut, regenerating-young forest, and mature forest were identified (Fig. 4). In 1995, the area consisted of 44.0% clear-cut, 28.4% regenerating young forest, and 27.6% mature forest, which correlated well with the findings of Hickey (1997). The initial age of each landcover type used in the simulation was 0-year (clear-cut), 20-years (regeneration) and 40-years (mature forest). Vegetation cover change is discussed further in Infinite Slope Model section.

Table 4
Vegetation parameters, their values and references showing the values

Parameter	Value used	Reference
Tree surcharge		
W_{max}, maximum (kPa)	[0.5, 2.5] uniform distribution	Hammond et al. (1992)
a_w, coefficient	0.952	Sidle (1991), Duan and Grant (2000)
b_w, coefficient	19.05	Sidle (1991), Duan and Grant (2000)
c_w, coefficient	−0.05	Sidle (1991), Duan and Grant (2000)
k_w, coefficient	0.12	Sidle (1991), Duan and Grant (2000)
Root strength		
R_{max}, maximum (kPa)	[2.97, 1.92] lognormal distribution	Hammond et al. (1992)
k_d, coefficient	0.402	Sidle (1991), Duan and Grant (2000)
n_d, coefficient	0.647	Sidle (1991), Duan and Grant (2000)
a_r, coefficient	0.952	Sidle (1991), Duan and Grant (2000)
b_r, coefficient	19.05	Sidle (1991), Duan and Grant (2000)
d_r, coefficient	−0.05	Sidle (1991), Duan and Grant (2000)
k_r, coefficient	0.12	Sidle (1991), Duan and Grant (2000)
Clear cut	0-year age	
Regeneration	20-year age	
Forest	40-year age	

3.3. SMR model: calibration

The SMR program first required a 60 to 90-day period of simulation to assure output was insensitive to the initial soil moisture content (Boll et al., 1998). An arbitrary 10% initial moisture content for the watershed was assigned (starting in July 1995). Our initial attempt using soil depth in Table 3 greatly over predicted peak discharges while the general stream flow curve was slightly lower than the observed curve. Because

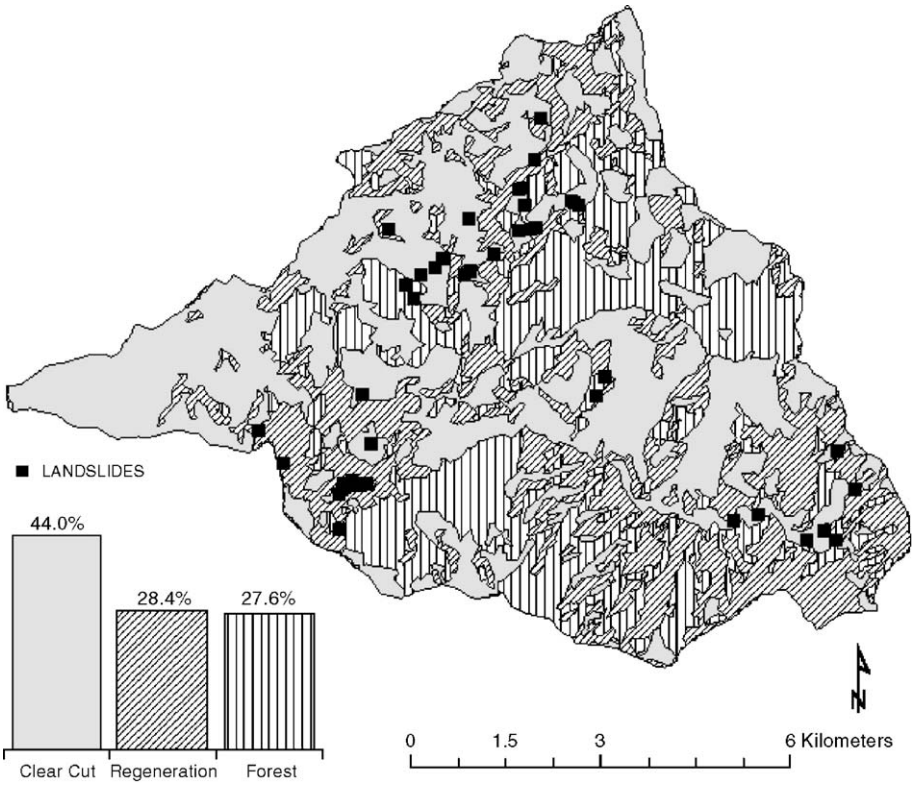

Fig. 4. Vegetation types in the Pete King watershed.

SSURGO provides soil depth up to 150 cm and the average values from the PDFs generated by the Monte Carlo simulation were used for assigning soil depths, the maximum values of the uniform distributions of soil depths were iteratively increased (by 10 cm increments) and re-run with the Monte Carlo simulations to improve the fit of the peaks and that of the general stream flow curves of the modeled and observed values. The number of quartiles used increased successively with iteration steps (i.e., for the first iteration we used quartile 4, for the second quartiles 4 and 3, for the third quartiles 4 to 2, and for the forth quartiles 4 to 1). The final soil depth values used in the SMR model ranged from 63 to 288 cm with a mean of 147 cm and standard deviation of 67 cm. Fig. 5 shows stream flow for the final calibrated model that was used for the 30-year simulation. Almost all stream discharge peaks were still slightly over-predicted by the SMR model, but the general fit of the model is in close agreement with the measured data.

3.4. Infinite slope model: input

Similar to Ward et al. (1982) and Duan and Grant (2000), the stochastic variables input to Eq. (8) were

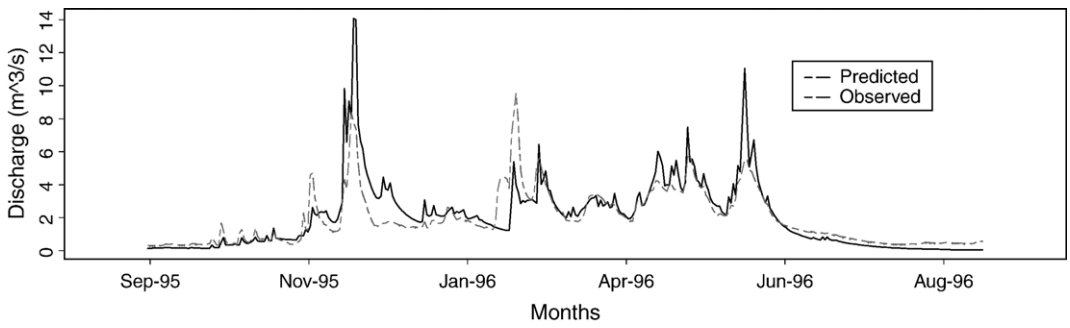

Fig. 5. Predicted versus observed stream flow for the Pete King watershed.

assumed to be independent and spatially distributed (Table 1). However, unlike FSmet and SHALSTAB, the SMR model dynamically simulates the saturated soil depth in space and time for each grid cell by inputting observed or predicted daily climate data into Eq. (1). Therefore, this GIS-based approach allows potential landslide-prone areas to be investigated through space and time. Input to the infinite slope model consisted of slope, soil depth, vegetation surcharge, and root strength.

Slope was derived using the finite difference formula. Gallant and Wilson (2000) showed that this formula gives better slope accuracy in comparison with other slope calculation approaches.

Soil depths determined for each horizon using the Monte Carlo simulation, which were used as multi-layer soils in the SMR module of the infinite slope model, were combined into a single soil layer for simplicity. Hammond et al. (1992) recommended a weighting method for adjusting the soil shear strength values when multiple soil layers are combined into a single layer. The values are adjusted to account for the shear strength along the entire failure plane. In this study, the soil shear strength values occurring in the base layer (B horizon) were given the highest weight (A horizon: 0.3; E horizon: 0.3; and B horizon: 0.4).

Vegetation surcharge was estimated using a sigmoidal function as suggested by Sidle (1987). The weight of the proportion of trees cut at the time of timber harvest is set to zero followed by an increase according to the function:

$$W = W_{\max}[(a_w + b_w e^{-k_w t})^{-1} + c_w] \quad (10)$$

where W is the vegetation surcharge at t years after cutting, $W_{\max}$ is the maximum vegetation surcharge, and a_w, b_w, c_w, and k_w are empirical constants. The function assumes uniform distribution of the tree surcharge across the area of interest, and the weight of the understory vegetation is assumed to be negligible (Sidle, 1992). The surcharge values for the coastal forest types of the US Pacific Northwest range from 1 to 5 kPa (O'Loughlin, 1974; Wu et al., 1979; Sidle, 1992). We used adjusted values between 0.5 and 2.5 kPa, which are more appropriate for the CNF (i.e., smaller size timber). Although the influence of vegetation surcharge on slope stability is small and often omitted from calculations (Hammond et al., 1992; Sidle, 1992), it was included because of its relation with the root strength and possible effect on the FS near the threshold of failure (Duan and Grant, 2000).

Root strength was determined following Sidle (1991), who modeled root cohesion during regeneration (R_r) and decaying residual root strength following harvest (R_d) using sigmoid and exponential curves, respectively:

$$R_r = R_{\max}[(a_r + b_r e^{-k_r t})^{-1} + d_r] \quad (11)$$

$$R_d = R_{\max} e^{-k_d t^{n_d}} \quad (12)$$

where a_r, b_r, d_r, and k_r are the regrowth constants, and n_d and k_d are the decay constants, derived by procedures outlined by Sidle (1991), t is the time increment, and $R_{\max}$ is the maximum root strength (Table 4).

Total root strength (R_{total}) is expressed as

$$R_{\text{total}} = R_r + R_d \quad (13)$$

$R_{\max}$ (2.97 kPa for the mean and 1.92 kPa for the variance; Table 4) was calculated using a lognormal probability distribution function for shallow soils and uncut forest with Monte Carlo simulation (Hammond et al., 1992).

4. Results and discussion

Results of the 30-year simulation are first compared to existing models (FSmet and SHALSTAB). Then the analysis of temporal prediction of landslide susceptibility is described, followed by the analysis of spatial prediction of landslide susceptibility.

4.1. Integrated approach versus existing models

The integrated modeling approach predicted landslide susceptibility with lower accuracy than FSmet and SHALSTAB, but with better precision based on the data and circumstances tested here. In this comparison, the ratio of correctly identified landslides to area

Table 5
Evaluation of SMR/FS/Monte Carlo, FSmet, and SHALSTAB models for the Pete King watershed with different cut-off values

Modeling technique	Area susceptible to landslides (%)		Correctly identified landslides (%)		Ratio
	(1)	(km^2)	(2)	(km^2)	(2/1)
SMR/FS/Monte Carlo ($p>0.5$)	8.1	5.6	20.0	0.008	2.47
SMR/FS/Monte Carlo ($p>0.7$)	4.5	3.1	11.1	0.005	2.47
SMR/FS/Monte Carlo ($p>0.9$)	1.5	1.0	2.2	0.001	1.47
SHALSTAB (cut-off>−2.2)	68.6	47.6	91.1	0.037	1.33
SHALSTAB (cut-off>−2.8)	44.5	30.9	62.2	0.025	1.40
SHALSTAB (cut-off>−3.1)	31.2	21.7	44.4	0.018	1.42
FSmet	14.0	9.7	20.0	0.008	1.43

susceptible to landslides was used as the criteria to evaluate the accuracy and precision of prediction of landslide susceptibility. Three different cut-off values were used for SMR/FS/Monte Carlo ($p>0.5$, $p>0.7$, $p>0.9$), and for SHALSTAB ($q/T>-2.2$, $q/T>-2.8$, $q/T>-3.1$). The values for the SMR/FS/Monte Carlo correspond to a landslide susceptibility on scale between 0 and 1, while those for SHALSTAB correspond to the nominal classes ("unconditionally stable," "potentially unstable," and "unconditionally unstable"). The output of the FSmet is a binary map delineating susceptible and stable areas. The output of the SMR/FS/Monte Carlo used a 30-year probability map for the comparison. Table 5 shows the validation of the model through the ratio values from the 1995 to 1996 landslide events. The ratio values show that SHALSTAB and FSmet more correctly identified landslides than SMR/FS/Monte Carlo, but SMR/FS/Monte Carlo

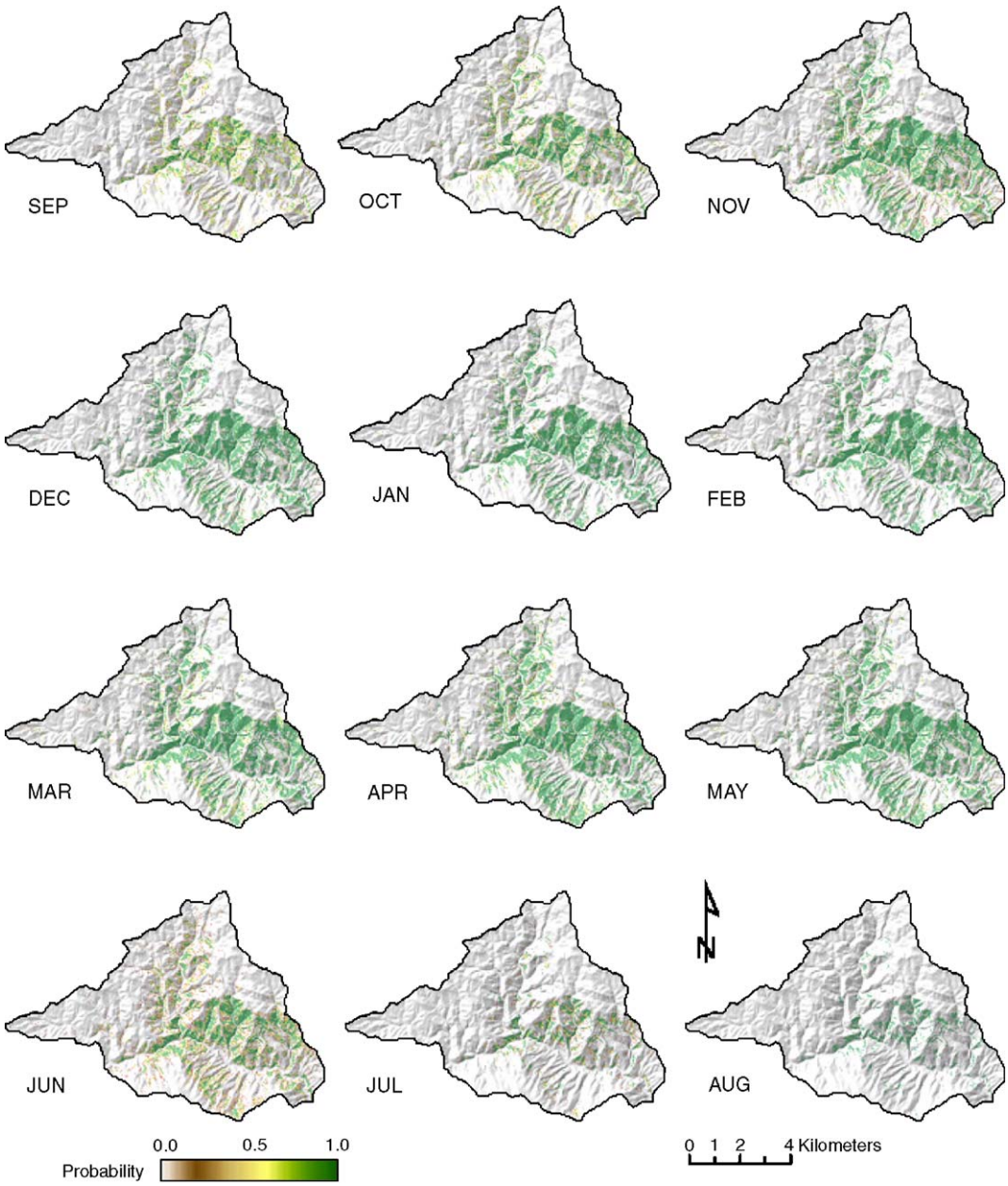

Fig. 6. Spatial patterns of monthly probability of landslide occurrence in the Pete King watershed for year 18.

method classifies a smaller percentage of the land area as susceptible. Consequently, the ratio values for SMR/FS/Monte Carlo are much higher than for SHALSTAB and FSmet.

However, the comparison here is intended to set a point of reference for the capabilities of the modeling approach, which is considerably different from the modeling approaches of SHALSTAB and FSmet. For example, year 18 in the simulation shows the highest percentage of landslide prone area. The monthly spatial patterns of landslide susceptibility are represented in Fig. 6. The percentage of susceptible area and that of correctly identified landslides vary during the year. For instance, using a monthly probability map for the comparison for a cut-off value of 0.9 in May a total of 19.5% area was classified as susceptible and 40.9% of the landslides were correctly predicted, while in the month of August a total of 3.7% was classified as susceptible and 9.1% of the landslides were correctly predicted. The ratio value for the month of May was 2.10 and the ratio value for August was 2.46. The percentage of correctly predicted landslides and the ratio value associated with month of May shows an improved accuracy and precision with the SMR/FS/Monte Carlo modeling approach.

4.2. Analysis of temporal prediction of landslide susceptibility

A *z*-test on the population of non-susceptible cells from the 30-year simulation confirmed that the number of susceptible and non-susceptible cells changed each year, at a significance level of 95% ($|3.798| > 1.96$). Time series plots of categorized probabilities of the number of landslide-prone cells in the Pete King watershed during the 30-year simulation period are shown in Fig. 7. These plots are arranged by the class of landslide probability, and have different *Y*-axis scales. The solid line represents a locally weighted regression fit known as Loess smoother to visualize time trends. Loess smoother is a curve-fitting technique based on local regression (Cleveland, 1993). The $p(0)$ plot shows that the number of stable cells increased through time. Plots of $p(0.1–0.2)$, $p(0.2–0.3)$, and $p(0.3–0.4)$ show a constant decrease of corresponding cells with time. The remaining plots with higher landslide susceptibility show an increase followed by a decrease, which is likely associated with the decrease of root strength after harvest and increase of root strength after regrowth through the simulation period.

The influence of root strength on the time trends and the effects of other important parameters suggested by previous studies (e.g., Hammond et al., 1992), including soil cohesion, internal friction angle, and soil depth, were further evaluated by sensitivity analysis. Table 6 shows the results obtained by altering one parameter while others were kept constant. For instance, by decreasing root strength by 1 kPa from the values used in the simulation, the susceptibility increased by ratio value of 0.19. When root strength was increased by 1 kPa the susceptibility to landslides decreased by a ratio value of 0.05. This implies that susceptibility increases with a higher rate when root strength is altered through harvesting. The sensitivity analyses suggest that the

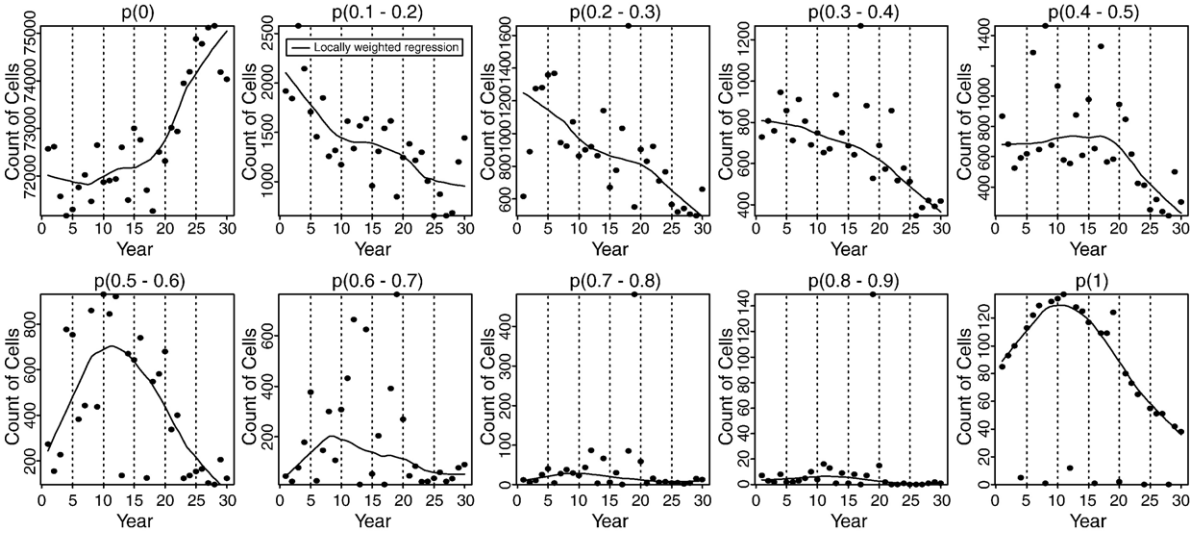

Fig. 7. Change in the number of cells prone to landslides for the 30-year simulation period.

Table 6
Sensitivity analysis of parameters used in the SMR/FS/Monte Carlo approach

Parameter	Value used	Area not susceptible to landslides (1) %	Incorrectly identified landslides (2) %	Ratio (2/1)
Soil cohesion				
	[0, 15] kPa	74.2	44.4	0.60
	+1 kPa	84.9	60.0	0.71
	+2 kPa	92.7	75.6	0.81
Internal friction angle				
	[27, 45] (°)	74.2	44.4	0.60
	+1°	76.8	46.7	0.61
	+2°	79.4	53.3	0.67
Root strength				
	−1 kPa	65.3	26.7	0.41
	[2,13] kPa	74.2	44.4	0.60
	+1 kPa	81.5	53.3	0.65
Soil depth				
	−10 cm	76.5	46.7	0.61
	[145, 69] cm	74.2	44.4	0.60
	+10 cm	72.2	40.0	0.55

increase in soil cohesion decreases susceptible areas with a higher rate than the increase in internal friction angle. Also, the analyses suggest that thicker soils increase susceptibility at a smaller rate than thinner soils. It should be noted that the effects of soil depth are also a function of slope, root cohesion, groundwater, and other variables as described by Hammond et al. (1992), and require additional testing to look at the interactions of these variables.

As expected, simulation results show that landslide susceptibility is a function of net precipitation and soil storage amount at different times during a year. Landslide susceptibility was low during dry periods (i.e., summer), and high during wet periods (i.e., spring). Spatial differences were caused by different groundwater levels and possibly by other patterns such as spatio-temporal rainfall distribution and snowmelt. The cumulative count of all cells with a FS < 1, for individual years during the simulation period shows that year 8 exhibited the largest number of susceptible cells, while year 28 exhibited the smallest number (Fig. 8). Year 8 is associated with neither the highest stream discharge nor the highest daily groundwater, but many small densely distributed rainfall events occurred in that year. This suggests that wet soils are prone to small and frequent events while dry soils could withstand large but less frequent events. However, high stream discharge was correlated with the count of cell susceptibility ($r = 0.75$) and daily water table depth ($r = 0.77$) for the simulation period. Fig. 9 shows a time series plot of the simulated stream flow from the watershed and the total volume of stream discharge in $m^3\ s^{-1}$ for each year, while Fig. 10 shows the count of cells predicted to be susceptible for the simulated period. These figures show the similarities in the patterns of the peak flow frequency and magnitude of events and verify the importance of watershed hydrology on landslide susceptibility through time.

Simulation results also show cell susceptibility decreased through time for the clear cut (CC), regeneration (REG), and the forest (FOR) vegetation classes, which is due to increased root strength in the absence of further disturbance. Fig. 11 shows a time series by vegetation class to represent probabilities of number of cells susceptible to landslides. The plot labeled CC $p(0)$ (non-susceptible cells) shows that a decrease was followed by an increase in non-susceptible

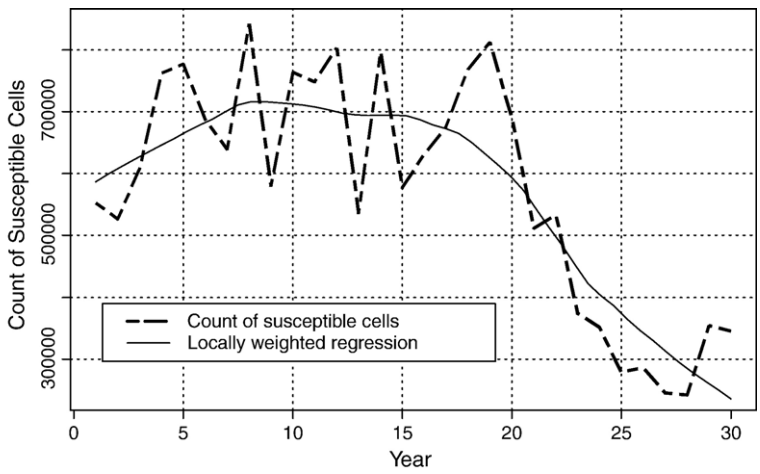

Fig. 8. Count of susceptible cells (FS <1) for each year during the 30-year simulation period in the Pete King watershed.

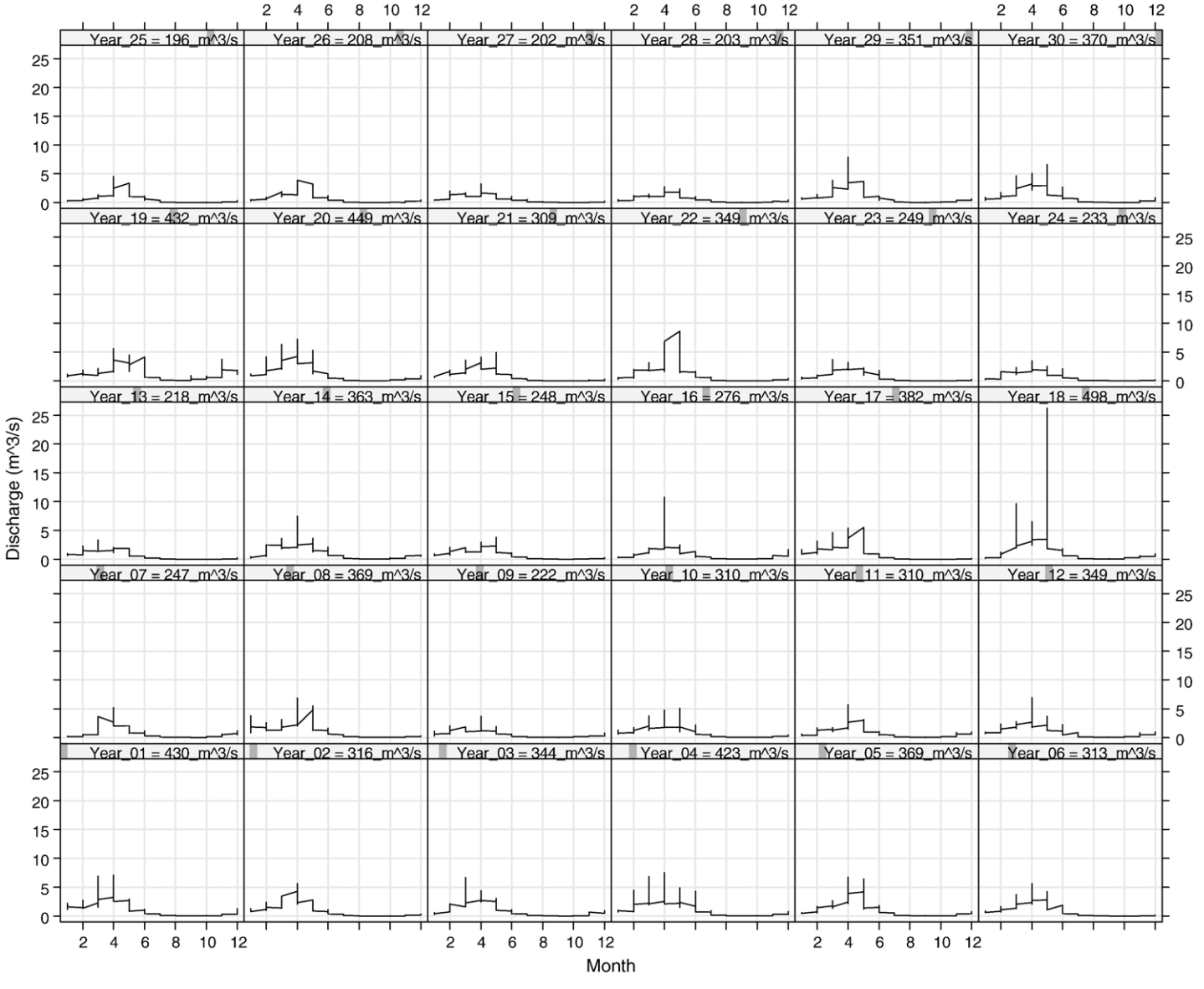

Fig. 9. Simulated stream flow for the Pete King watershed during the 30-year simulation period.

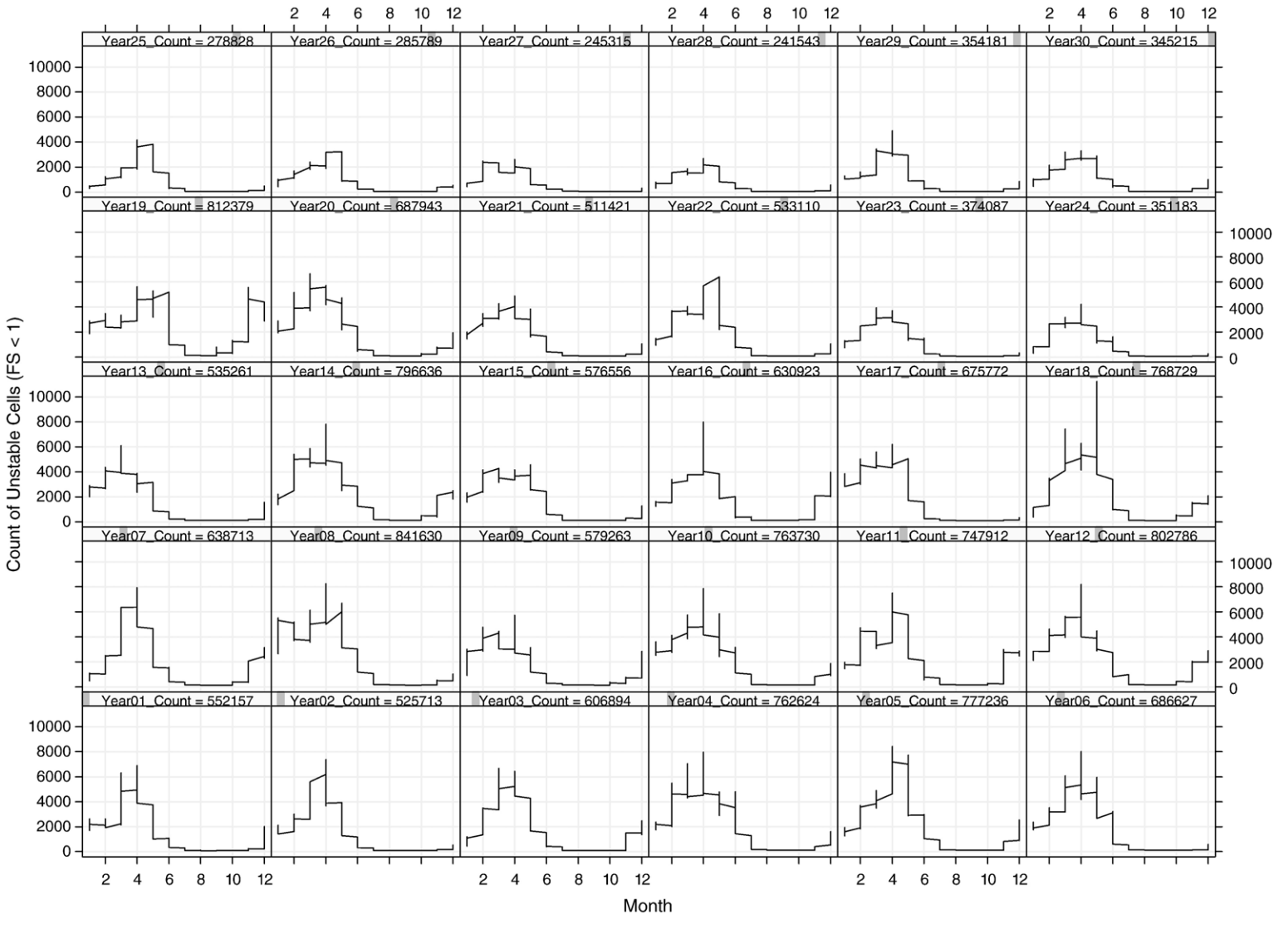

Fig. 10. Simulated landslide susceptibility for the Pete King watershed during the 30-year simulation period.

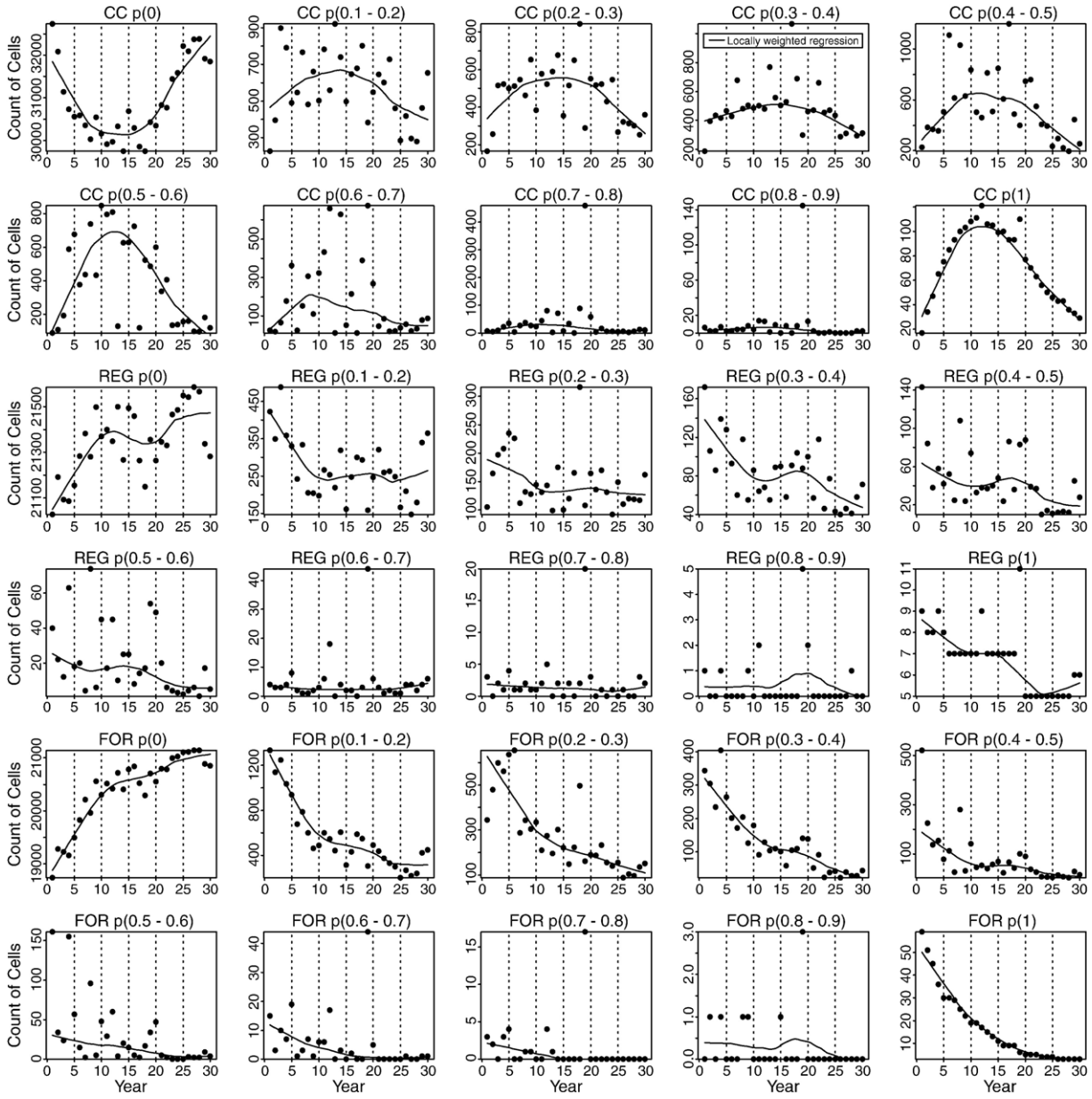

Fig. 11. Change in the number of cells susceptible to landslides by vegetation classes for the 30-year simulated period.

areas with the maximum susceptibility in years 12 to 13 when root strength was weakest, while the REG $p(0)$ and FOR $p(0)$ show constant increase in non-susceptible areas. The trends for the clear cuts suggest that the susceptibility is high when root decaying reaches its maximum while the dip in the locally weighted regression in REG $p(0)$ and FOR $p(0)$ may suggest that susceptibility for older vegetation types is driven more likely by the frequency and the magnitude of events (Figs. 9 and 10). Therefore, susceptibility associated with vegetation types in long-term planning should be considered and differentiated between different vegetation types.

4.3. Analysis of spatial prediction of landslide susceptibility

Comparison of the spatial changes of the FS for the study area showed that the location of non-susceptible cells changed over the 30-year simulation as well as during individual years, and was controlled by topography, soil moisture, and vegetation patterns.

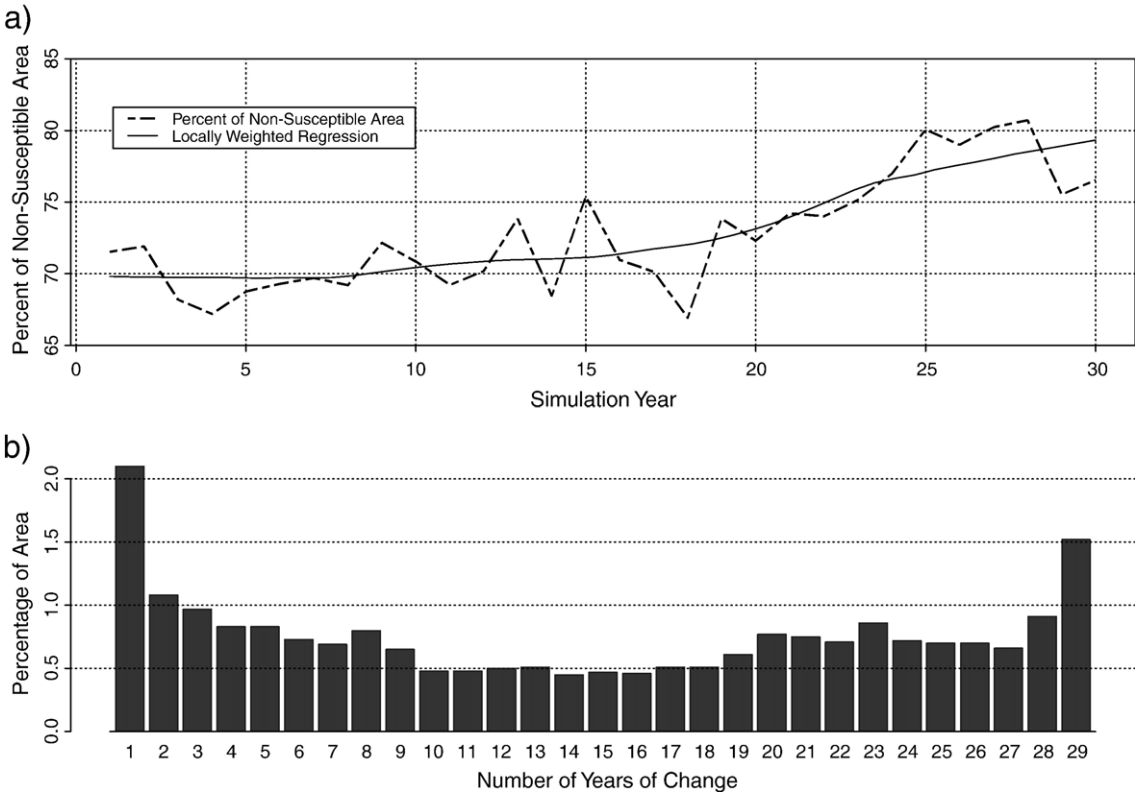

Fig. 12. Spatial change in (a) percent of non-susceptible area within the Pete King watershed for the 30-year simulation period, and (b) the number of years with FS <1 events given in percentage of area.

Fig. 12a shows that year 28 exhibits the largest area of non-susceptible cells, while year 18 exhibits the largest area of susceptible cells. Also, in Fig. 12a, the trend of a locally quadratic regression shows that the area not susceptible to landslides increased through time. Fig. 12b shows the areal percentage of cells according to the number of years with at least one event of FS <1. It shows that 2.1% of the cells have only one year of FS <1, while 1.5% of the cells have all (29) years with FS <1. Fig. 13 shows that vegetation types influence the spatial distribution of the FS. The clear-cut line in Fig. 13 shows that susceptibility increases and reaches its maximum in year 18 before it starts to decrease again. The other vegetation types show a constant decrease of susceptibility through time. It is also interesting that years 13 and 15 show a rapid decrease in susceptibility for all vegetation types, which is reflected through the low amount of stream flow (Fig.

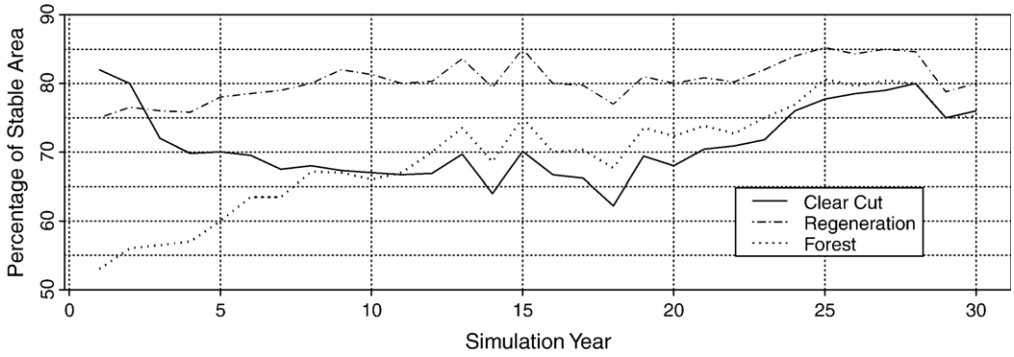

Fig. 13. Change in percentage of areas of non-susceptible cells covered by different vegetation types.

9). The largest susceptible area is associated with year 18, which is due to the largest single event shown in Fig. 9. However, the largest susceptible area for year 18 does not coincide with the year that experienced the most unstable cells (Fig 10). This implies that a single large event that can saturate the soil influences susceptibility in space to a large extent, while frequent small events when the soil has been saturated can influence susceptibility in time as well as in space.

Comparisons of spatial changes for individual months for the most landslide prone year (18) show that the month of May had the largest percentage of susceptible area (33.2%) while August had the least (3.8%). The patterns of change in year 18 (Fig. 6) appear to be largely controlled by topography and soil moisture. Soil moisture influence was supported by the high correlation between the count of susceptible cells and water table depth ($r=0.89$) as well as stream discharge ($r=0.80$). Visual inspection of Fig. 6 also suggests that topographically convergent areas had the highest probability of landslide occurrence. These areas expanded when they received more moisture from rain, snowmelt, or lateral flow from adjacent cells.

5. Summary and conclusions

A dynamic, distributed GIS based model, was presented to evaluate spatial and temporal slope instability on a watershed scale. The model integrates the SMR model, the infinite slope model, Monte Carlo simulation, and continuous changes in vegetation surcharge and root strength. The model was first calibrated with observed daily climate and stream flow data for the year with actual landsliding, before it was used to simulate spatial and temporal landslide susceptibility for a 30-year period. Dynamic factors (e.g., root strength, vegetation surcharge) were included using Monte Carlo simulation with stochastically derived long-term climatic inputs. This approach is based on a limited sampling of landslide events. The use of theoretical distributions of some parameters is an attempt to explicitly increase detailed mapping information in remote areas susceptible to landslides.

The obtained spatial landslide prediction offered significant improvements over the existing models (FSmet and SHALSTAB) by incorporating temporal resolution and extending capabilities to simulate long-term land-use scenarios. The model application showed FS is influenced by the dynamics of root strength in space and time, which was supported by sensitivity analysis. In particular, the influence of root strength on landslide susceptibility is greater for clear cuts while other vegetation types are influenced mostly by the frequency and magnitude of the events. The results also showed that the years with the highest spatial and temporal instability are not the same. The year with the highest temporal instability was driven by frequent and smaller rainfall events, while the year with the highest spatial instability was driven by the largest single rainfall and stream flow event.

The results from the integrated approach are promising for management applications and decision-making in remote areas where detailed information about the distributed parameters is unavailable. The proposed methodology could incorporate parameters with various levels of uncertainties. Although better quantification of the uncertainty and a more accurate representation of spatial and temporal parameter variability may be possible, the intention here was to show a quantitative unbiased approach in distributing uncertainties to investigate slope stability in space and time. As demonstrated, land-use through timber harvesting affects slope stability, so this methodology could be further extended to incorporate disturbance events such as a severe wildfire or insect infestation to reset conditions for mapping landslide susceptibility. However, further testing of the model including field verification and additional sensitivity analysis is recommended.

Acknowledgement

This work was supported though data provided by the Clearwater National Forest and the Rocky Mountain Research Station in Moscow, Idaho. The authors would also like to thank Dr. Oliver Korup and Dr. Kevin M. Schmidt for their comments, as well as Dr. Takashi Oguchi, who provided helpful suggestions and editorial assistance.

References

Ayalew, L., Yamagishi, H., 2005. The application of GIS-based logistic regression for landslide susceptibility mapping in the Kakuda-Yahiko Mountains, Central Japan. Geomorphology 65, 15–31.

Beven, K., Kirkby, M.J., 1979. A physically based, variable contributing area model of basin hydrology. Hydrological Sciences Bulletin 24, 43–69.

Blöchl, A., Braun, B., 2005. Economic assessment of landslide risks in the Swabian Alb, Germany—research framework and first results of homeowners' and experts' surveys. Natural Hazards and Earth System Sciences 5, 389–396.

Boll, J., Brooks, E.S., Campbell, C.R., Stockle, C.O., Young, S.K., Hammel, J.E., McDaniel, P.A., 1998. Progress toward development of a GIS based water quality management tool for small rural watersheds: modification and application of a distributed model.

ASAE Annual International Meeting in Orlando, Florida, July 12–16, Paper 982230, ASAE, 2950 Niles Road, St. Joseph, MI 49085-9659, USA.

Bresler, E., Russo, D., Miller, R.D., 1978. Rapid estimate of unsaturated hydraulic conductivity function. Soil Science Society of America Proceedings 42, 170–172.

Burrough, P.A., McDonnell, R.A., 1998. Principles of Geographic Information Systems. Oxford University Press, Oxford.

Burton, A., Bathurst, J.C., 1998. Physically based modelling of shallow landslide sediment yield at a catchment scale. Environmental Geology 35, 89–99.

Carrara, A., 1983. Multivariate models for landslide hazard evaluation. Mathematical Geology 15, 402–426.

Carrara, A., Cardinali, M., Detti, R., Guzzetti, F., Pasqui, V., Reichenbach, P., 1991. GIS techniques and statistical models in evaluating landslide hazard. Earth Surface Processes and Landforms 16, 427–445.

Carrara, A., Cardinali, M., Guzzetti, F., Reichenbach, P., 1995. GIS technology in mapping landslide hazard. In: Carrara, A., Guzzetti, F. (Eds.), Geographical Information Systems in Assessing Natural Hazards. Kluwer Academic Publishers, Dordrecht, pp. 135–175.

Chung, C.F., Fabbri, A.G., 1999. Probabilistic prediction model for landslide hazard mapping. Photogrammetric Engineering and Remote Sensing 65, 1389–1399.

Chung, C.F., Fabbri, A.G., van Westen, C.J., 1995. Multivariate regression analysis for landslide hazard zonation. In: Carrara, A., Guzzetti, F. (Eds.), Geographical Information Systems in Assessing Natural Hazards. Kluwer Academic Publishers, Dordrecht, pp. 107–133.

Cleveland, W.S., 1993. Visualizing Data, Summit. Hobart Press, New Jersey.

CRED, 2006. EM-DAT: The OFDA/CRED International Disaster Database. Université Catholique de Louvain, Brussels, Belgium, http://www.em-dat.net/.

Dietrich, W.E., Montgomery, D.R., 1998. SHALSTAB: a digital terrain model for mapping shallow landslide potential. National Council of the Paper Industry for Air and Stream Improvement. Technical Report.

Dietrich, W.E., Reiss, R., Hsu, M.L., Montgomery, D.R., 1995. A process-based model for colluvial soil depth and shallow landsliding using digital elevation data. Hydrological Processes 9, 383–400.

Dhakal, A.S., Amada, T., Aniya, M., 2000. Landslide hazard mapping and its evaluation using GIS: an investigation of sampling schemes for a grid-cell based quantitative method. Photogrammetric Engineering and Remote Sensing 66, 981–989.

Duan, J., Grant, G.E., 2000. Shallow landslide delineation for steep forest watersheds based on topographic attributes and probability analysis. In: Wilson, J.P., Gallant, J.C. (Eds.), Terrain Analysis: Principles and Applications. John Wiley & Sons, Inc., New York, pp. 311–329.

Flanagan, D.C., Livingston, S.J., 1995. WEPP user summary. NSERL Report No. 11, W. Lafayette. National Soil Erosion Research, p. 131.

Forest Service Clearwater National Forest (FS-CNF), 1983. Land System Inventory. ID, Orofino.

Frankenberger, J.R., Brooks, E.S., Walter, M.T., Walter, M.F., Steenhuis, T.S., 1999. A GIS-based variable source area hydrology model. Hydrological Processes 13, 804–822.

Gallant, J.C., Wilson, J.P., 2000. Primary topographic attributes. In: Wilson, J.P, Gallant, J.C. (Eds.), Terrain Analysis Principles and Applications. John Wiley & Sons, Inc., New York, pp. 51–85.

Gessler, P.E., Moore, I.D., McKenzie, N.J., Ryan, P.J., 1995. Soil-landscape modelling and spatial prediction of soil attributes. International Journal of Geographic Information Systems 9, 421–432.

Gessler, P.E., Chadwick, O.A., Chamran, F., Althouse, L., Holmes, K., 2000. Modeling soil-landscape and ecosystem properties using terrain attributes. Soil Science Society of American Journal 64, 2046–2056.

Glade, T., 1998. Establishing the frequency and magnitude of landslide-triggering rainstorm events in New Zealand. Environmental Geology 35, 160–174.

Gorsevski, P.V., 2002. Landslide hazard modeling using GIS. Ph.D. Dissertation, University of Idaho, Moscow, USA.

Gorsevski, P.V., Gessler, P.E., Foltz, R.B., 2000. Spatial prediction of landslide hazard using logistic regression and GIS. 4th International Conference on Integrating GIS and Environmental Modeling (GIS/EM4): Problems, Prospects and Research Needs, Banff, Alberta, Canada, September 2–8, 2000.

Gorsevski, P.V., Gessler, P.E., 2003. Bayesian modeling and GIS for evaluating landslide hazard. ASPRS 2003 Annual Conference, Anchorage, AK, May 5–9, 2003.

Gorsevski, P.V., Gessler, P.E., Jankowski, P., 2003. Integrating a fuzzy k-means classification and a Bayesian approach for spatial prediction of landslide hazard. Journal of Geographical Systems 5, 223–251.

Gorsevski, P.V., Jankowski, P., Gessler, P.E., 2005. Spatial prediction of landslide hazard using fuzzy k-means and Dempster–Shafer theory. Transactions in GIS 9, 455–474.

Guzzetti, F., Reichenbach, P., Cardinali, M., Galli, M., Ardizzone, F., 2005. Probabilistic landslide hazard assessment at the basin scale. Geomorphology 72, 272–299.

Hargreaves, G.H., Samani, Z.A., 1985. Reference crop evapotranspiration from temperature. Applied Engineering in Agriculture 1, 96–99.

Hammond, C., Hall, D., Miller, S., Swetik, P., 1992. Level I Stability Analyses (LISA) Documentation for Version 2.0. Gen. Tech. Rep. INT-285. U.S. Department of Agriculture, Forest Service, Intermountain Research Station, Ogden, UT, p. 190.

Hickey, R., 1997. Evaluating the WATBAL sediment loading model, Clearwater National Forest, Idaho. Northwest Science 71, 233–242.

Malczewski, J., 1999. GIS and Multicriteria Decision Analysis. John Wiley & Sons, Inc., New York, NY.

Mark, R.K., Ellen, S.D., 1995. Statistical and simulation models for mapping debris-flow hazard. In: Carrara, A., Guzzetti, F. (Eds.), Geographical Information Systems in Assessing Natural Hazards. Kluwer Academic Publishers, Dordrecht, pp. 93–106.

McClelland, D.E., Foltz, R.B., Wilson, W.D., Cundy, T.W., Heinemann, R., Saurbier, J.A., Schuster, R.L., 1997. Assessment of the 1995 1996 floods and landslides on the Clearwater National Forest: Part I. Landslide Assessment. A Report to the Regional Forester Northern Region U.S. Forest Service, December.

Moore, I.D., Grayson, R.B., Ladson, A.R., 1991. Digital terrain modelling—a review of hydrological, geomorphological and biological applications. Hydrological Processes 5, 3–30.

Montgomery, D.R., Dietrich, W.E., 1994. A physically based model for the topographic control on shallow landsliding. Water Resources Research 30, 1153–1171.

Moreiras, S.M., 2005. Landslide susceptibility zonation in the Rio Mendoza Valley, Argentina. Geomorphology 66, 345–357.

National Oceanic and Atmospheric Administration, 2001. Climatological Data, Idaho, Fenn Ranger Station. Accessed 20 November 2001, http://www.noaa.gov/.

Nicks, A.D., Lane, L.J., Gander, G.A., 1995. Chapter 2. Weather generator. In: Flanagan, D.C., Nearing, M.A. (Eds.), USDA-Water Erosion Prediction Project Hillslope Profile and Watershed Model Documentation, W. Lafayette, IN: USDA Agricultural Research Service 2.1-2.22.

Okimura, T., Ichikawa, R., 1985. A prediction method for surface failures by movements of infiltrated water in a surface soil layer. Natural Disaster Science 7, 41–51.

O'Loughlin, C.L., 1974. A study of tree root strength deterioration following clear felling. Canadian Journal of Forest Research 4, 107–113.

O'Loughlin, E.M., 1986. Prediction of surface saturation zones in natural catchments by topographic analysis. Water Resources Research 22, 794–804.

Quinn, P., Beven, K.J., Chevallier, P., Planchon, O., 1991. The prediction of hillslope flow paths for distributing hydrological modelling using digital terrain models. Hydrological Processes 5, 59–79.

Saxton, K.E., Rawls, W.J., Romberger, J.S., Papendick, R.I., 1986. Estimating generalized soil–water characteristics from texture. Soil Science Society of American Journal 50, 1031–1036.

Sidle, R.C., 1987. A dynamic model of slope stability in zero-order basins. IAHS Publication 165, 101–110.

Sidle, R.C., 1991. A conceptual model of changes in root cohesion in response to vegetation management. Journal of Environmental Quality 20, 43–52.

Sidle, R.C., 1992. A theoretical model of the effects of timber harvesting on slope stability. Water Resources Research 28, 1897–1910.

Thornthwaite, C.W., Mather, J.R., 1955. The Water Balance. Laboratory of Climatology, Publ. No. 8, Centerton NJ.

U.S. Army Corps of Engineers, 1960. Engineering and Design: Runoff from Snowmelt. EM 1110-2-1406.

U.S. Department of Agriculture (USDA) Natural Resources Conservation Service (NRCS), 2001. Soil Survey Geographic Database (SSURGO), Kooskia Area, Idaho County, ID. Accessed 7 November 2001, http://www.ftw.nrcs.usda.gov/stssaid.html.

Ward, T.J., Li, R., Simons, D.B., 1982. Mapping landslide hazard in forest watersheds. Transactions of the American Society of Civil Engineers 108, 319–324.

Wu, W., Sidle, R.C., 1995. A distributed slope stability model for steep forested basins. Water Resources Research 31, 2097–2110.

Wu, T.H., McKinnell, W.P., Swanston, D.N., 1979. Strength of tree roots and landslides on Prince of Wales Island, Alaska. Canadian Geotechnical Journal 16, 9–33.